of terrestrial, synthetic, and lunar ilmenites. *Earth and Planetary Science Letters*, **26**: 377–386.

Smirnov, A.V., and Tarduno, J.A., 2002. Magnetic field control of the low-temperature magnetic properties of stoichiometric and cation-deficient magnetite. *Earth and Planetary Science Letters*, **194**: 359–368.

Snowball, I., and Torii, M., 1999. Incidence and significance of magnetic iron sulphides in Quaternary sediments and soils. In Maher, B.A., and Thompson, R. (eds.), *Quaternary Climates, Environments and Magnetism.* Cambridge: Cambridge University Press, pp. 199–230.

Strangway, D.W., Honea, R.M., McMahon, B.E., and Larson, E.E., 1968. The magnetic properties of naturally occurring goethite. *Geophysical Journal of the Royal Astronomical Society*, **15**: 345–359.

Syono, Y., 1965. Magnetocrystalline anisotropy and magnetostriction of Fe_3O_4–Fe_2TiO_4 series—with special application to rocks magnetism. *Japanese Journal of Geophysics*, **4**: 71–143.

Taylor, R.M., and Schwertmann, U., 1974. Maghemite in soils and its origin. I. Properties and observations on soil maghemites. *Clay Minerals*, **10**: 289–298.

Thorpe, A.N., Minkin, J.A., Senftle, F.E., Alexander, C., Briggs, C., Evans, H.T. Jr., and Nord, G.L. Jr., 1977. Cell dimensions and antiferromagnetism of lunar and terrestrial ilmenite single crystals. *Journal of Physics and Chemistry of Solids*, **38**: 115–123.

Tucker, P., 1981. Low-temperature magnetic hysteresis properties of multidomain single-crystal titanomagnetite. *Earth and Planetary Science Letters*, **54**: 167–172.

Uyeda, S., 1958. Thermo-remanent magnetism as a medium of palaeomagnetism, with special reference to reverse thermo-remanent magnetism. *Japanese Journal of Geophysics*, **2**: 1–123.

van der Lugt, W., and Poulis, N.J., 1961. The splitting of the nuclear magnetic resonance lines in vivianite. *Physica*, **27**: 733–750.

Verwey, E.J.W., 1939. Electronic conduction of magnetite (Fe_3O_4) and its transition point at low temperatures. *Nature*, **44**: 327–328.

Verwey, E.J.W., and Haayman, P.W., 1941. Electronic conductivity and transition point of magnetite ("Fe_3O_4"). *Physica*, **8**: 979–987.

Walz, F., 2002. The Verwey transition—a topical review. *Journal of Physics: Condensed Matter*, **14**: R285–R340.

Weiss, P., and Forrer, R., 1929. La saturation absolue des ferromagnétiques et les lois d'approche en fonction du champ et de la température. *Annales de Physique*, 10^e série, **12**: 279–374.

Weiss, P., and Renger, K., 1914. Die anfängliche Permeabilität von Eisen und Magnetit in Funktion der Temperatur und die Abhängigkeit der Umwandlungspunkte von der Feldstärke. *Archiv für Electrotechnik*, **2**: 406–418.

Zergenyi, R.S., Hirt, A.M., Zimmermann, S., Dobson, J.B., and Lowrie, W., 2000. Low-temperature magnetic behavior of ferrihydrite. *Journal Geophysical Research*, **105**: 8297–8303.

Cross-references

Iron Sulfides
Magnetic Mineralogy, Changes due to Heating
Magnetic Proxy Parameters
Rock Magnetism
Rock Magnetism, Hysteresis Measurements

MAGNETIC PROXY PARAMETERS

Introduction

As a rule, a natural system is complex and the result of the interplay of numerous constituting parameters. To fully describe such systems, ideally each (independent) parameter must be known. However, their mere number would imply a substantial analytical operation and in practice one should look for parameters that describe the essential parts of the system. Because these parameters can only describe the system in an approximate fashion they are termed "proxy parameters" or "proxies." There exists a myriad of proxies including the chemical analysis of inorganic or organic compounds, the number and types of living and fossil biota, and the physical properties of a sample, such as grain-size distribution, porosity, magnetic properties, etc. Basically, each physical, chemical, or biological parameter that is measurable reasonably quickly at reasonable cost may serve as proxy to describe a complete system. One should realize that up to over several thousands of data points are rapidly gathered in a case study. Combinations of two or more of those parameters may yield valuable proxies as well. Another important condition for a parameter to serve as proxy is that its meaning must be understood. This pertains to the analytical point of view as well as to its functioning in the natural system. In the following, we outline the merit and potential of the so-called mineral-magnetic proxies.

From the analytical viewpoint, the assets of mineral-magnetic or rock-magnetic proxy parameters are manifold. They include sensitivity, rapidity, ease of sample preparation, comparatively modestly priced instrumentation for data acquisition, nondestructiveness, and in particular the ability to sense grain-size variation in the ultrafine grain-size range. Magnetic properties refer to bulk sample properties in contrast to (electron) microscopical techniques where often only a small fraction of a sample can be analyzed. Therefore, mineral-magnetic parameters are well suited as proxy parameters. As drawbacks should be mentioned that some of the parameters are nonunique, and that their scales are most often utilized in a relative sense. Often ratios of several parameters are used to reduce nonuniqueness. The meaning of a ratio may change depending on the absolute values of numerator and denominator; hence, may vary among case studies. Proper interpretation of a mineral-magnetic data set therefore requires expert training and a feel for potential variability in the data cloud.

Magnetism

Mineral-magnetic parameters refer to the concentration and properties of iron oxides (and some iron sulfides), minerals that occur in trace amounts in any rock, soil, or even organic tissue. In quantum mechanics, electrons are assigned orbital and spin magnetic moments. For magnetism, the spin moment is most important: each electron can be regarded as a microscopic magnet. In most compounds electrons act independently and consequently a very low-magnetic moment is measured in applied magnetic fields and no permanent or remanent magnetic moment can exist. This is the case in diamagnetic and paramagnetic substances. Diamagnetism—occurring in compounds with no unpaired electron spins—is characterized by a small but negative magnetic moment in applied fields. It is a property of all matter because all paired electrons yield a diamagnetic moment. Paramagnetism—characteristic of compounds with unpaired electron spins—yields a positive magnetic moment that outweighs diamagnetic moments very quickly.

By virtue of exchange interaction, a property described also by quantum mechanics, the outermost electrons of transition elements may act collectively in some compounds, provided that their orbitals sufficiently overlap. For the first row transition elements, this situation occurs in metal oxides. In nature, iron is the most important element and the collective electron behavior is termed ferromagnetism (*sensu lato*). Several classes of ferromagnetism are distinguished: ferromagnetism, ferrimagnetism, and antiferromagnetism (Figure M48).

Ferromagnetic and ferrimagnetic materials have very large magnetic moments in applied fields, several orders of magnitude larger than a typical paramagnet. Antiferromagnetic materials ideally would have a net magnetic moment of zero but in reality usually a weak moment persists. Collective spin behavior gives rise to the existence of permanent or remanent magnetization, i.e., magnetic moments that remain after removal of an external magnetic field. The magnetic properties

of ferromagnets (*sensu lato*) are dependent on mineral type, temperature, grain size, and strain state of the grain. Subtle variations in magnetic properties can thus be interpreted in terms of changing concentration, grain size, or strain state of the magnetic materials. In a geoscientific context, in turn, these can be interpreted along the lines of changes in catchment area, in climate, in diagenesis, or in oxidation degree when dealing with a series of lava flows. This is exploited when utilizing magnetic properties as proxy parameters.

Magnetic minerals

In nature, magnetic minerals are largely restricted to iron–titanium oxides that may contain minor amounts of substituted aluminum, chromium, manganese, and magnesium. The most important terrestrial magnetic mineral is magnetite (Fe_3O_4), one of the endmembers of the titanomagnetite solid-solution series (the other endmember is ulvöspinel, Fe_2TiO_4). Hematite (α-Fe_2O_3) is another important mineral; it is one of the endmembers of the titanohematite solid-solution series (the other endmember is ilmenite, $FeTiO_3$). Goethite (α-FeOOH), pyrrhotite (Fe_7S_8), and greigite (Fe_3S_4) are often referred to as minor magnetic minerals. Some copper minerals show magnetic properties as well but their occurrence is restricted to certain iron types. Metallic iron is very rare in terrestrial environments but occurs prominently in meteorites. Magnetic minerals can be distinguished from each other by their Curie point temperature, the temperature above which collective behavior is lost and a paramagnetic substance remains. When dealing with antiferromagnetic minerals the temperature at which collective behavior is lost, is referred to as Néel point temperature. In practice Curie and Néel temperature are used interchangeably. When cooling below the Curie or Néel temperature, collective spin coupling sets in again. For most magnetic minerals the Curie (Néel) temperature is several hundreds of degree Celsius, i.e., far above room temperature (see Table M2). If we would extend the measurement range down to a few Kelvin, many silicate minerals will order magnetically as well. However, this is not routinely done because it requires specific instrumentation that is not widely available.

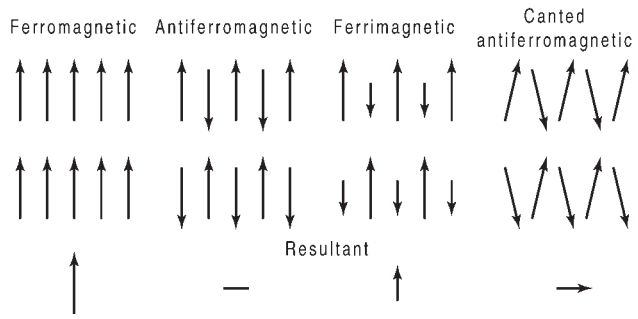

Figure M48 Classes of magnetism. The resultant magnetic moment is indicated below.

Grain-size indicators

Small grains have a different number of magnetic domains—zones with a uniform magnetization direction within a grain—than large grains of the same magnetic mineral. Hence, magnetic properties that reflect somehow the number of domains, are grain-size indicative. From the smallest grain size to the largest, four main domain structure types are distinguished: superparamagnetic, single-domain, pseudosingle-domain, and multidomain (Figures M49 and M50). The boundaries between these domain types are gradual, but the change in domain-state dependent properties essentially forms a continuum. Superparamagnetic grains are that small that they cannot support a stable domain configuration: upon a changing external field the spin configuration

Table M2 Some natural magnetic minerals, Curie (T_C) or Néel temperature (T_N) and magnetic structure below T_C or T_N. More detailed descriptions of the magnetic properties of most of these phases are given by Hunt *et al.* (1995), Dunlop and Özdemir (1997), Maher and Thompson (1999), or Evans and Heller (2003)

Mineral name	Composition	T_C or T_N	Magnetic structure
Magnetite–ulvöspinel	Fe_3O_4–Fe_2TiO_4	578 °C to –155 °C	Ferrimagnetic
Magnetite–hercynite	Fe_3O_4–$FeAl_2O_4$	578 °C to 339 °C	Ferrimagnetic
Magnetite–jacobsite	Fe_3O_4–Fe_2MnO_4	578 °C to 350 °C	Ferrimagnetic
Magnetite–chromite	Fe_3O_4–Fe_2CrO_4	578 °C to 30 °C	Ferrimagnetic
Hematite–ilmenite	α-Fe_2O_3–$FeTiO_3$	675 °C to –170 °C	Canted antiferromagnetic–ferrimagnetic[a]
Maghemite	γ-Fe_2O_3	645 °C[b]	Ferrimagnetic
Goethite	α-FeOOH	120 °C	Antiferromagnetic
Akagenéite	β-FeOOH	26 °C	Antiferromagnetic
Bernallite	$Fe(OH)_3$	154 °C	Canted(?) antiferromagnetic[c]
Feroxyhite	δ'-FeOOH	177 °C	Ferrimagnetic
Pyrrhotite	Fe_7S_8–$Fe_{11}S_{12}$	325 °C	Ferrimagnetic–antiferromagnetic[d]
Greigite	Fe_3S_4	350 °C ?[e]	Ferrimagnetic
Iron	Fe	770 °C	Ferromagnetic
Lepidocrocite	γ-FeOOH	–196 °C	Antiferromagnetic[f]
Siderite	$FeCO_3$	–238 °C	Antiferromagnetic[f]
Ferrihydrite	$Fe_5HO_8{\cdot}4H_2O$	–158 °C to –248 °C[f]	Speromagnetic[f,g]

[a]Above the Morin transition, hematite has a canted antiferromagnetic structure which results in a macroscopic magnetic moment, its structure becomes ferrimagnetic with increasing Ti-content. As in the titanomagnetite solid-solution series, high Ti-contents yield Curie temperatures below room temperature.
[b]Most maghemites invert to hematite before their Curie temperature is reached.
[c]The structure of bernallite is not known with certainty.
[d]Only monoclinic pyrrhotite (Fe_7S_8) is ferrimagnetic at room temperature, the other pyrrhotite structures become ferrimagnetic on heating above ~200 °C.
[e]On heating, greigite decomposes before it reaches its Curie temperature. Therefore, the temperature listed should be regarded with great caution.
[f]The last three minerals listed are paramagnetic at room temperature but they order magnetically at low temperatures, so their presence can be demonstrated with magnetic methods. Furthermore, on heating a sample above room temperature these paramagnetic minerals chemically alter into magnetic minerals.
[g]Speromagnetism is characterized by short-range antiferromagnetic spin coupling. On longer ranges the magnetic ordering is random. The range of ordering temperatures of ferrihydrite is related to its crystallinity.

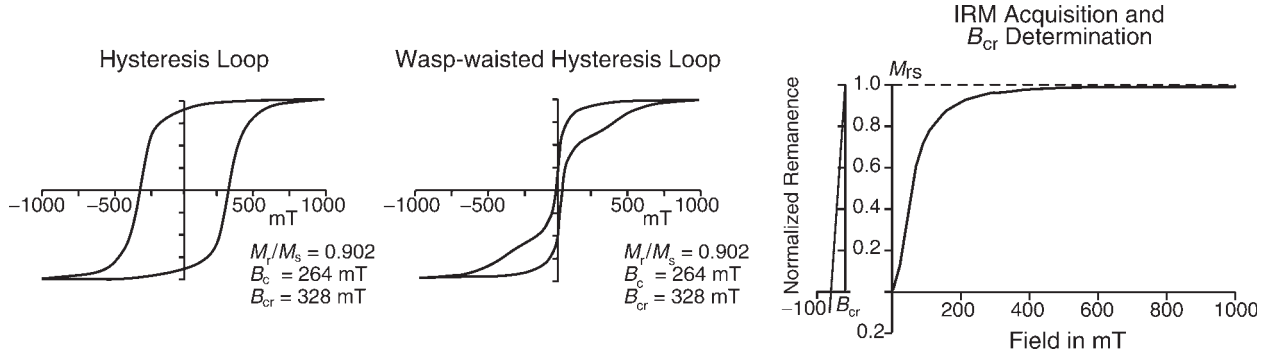

Figure M49 Examples of magnetic hysteresis loops (left, central). (*Left*) Hysteresis loop of an ensemble of single-domain grains. Single-domain grains are characterized by square hysteresis loops; loops of pseudosingle-domain and multidomain grains are increasingly slender and have inclined slopes. (*Central*) So-called "wasp-waisted" hysteresis loop. The central section is smaller than the outer parts. Wasp-waisted loops are typically of mixed ensembles with contrasting coercivities: either a mixture of two magnetic minerals (magnetite and hematite in the present case) or a mixture of superparamagnetic and larger grains of the same mineral. (*Right*) Determination of an IRM acquisition curve and the remanent coercive force.

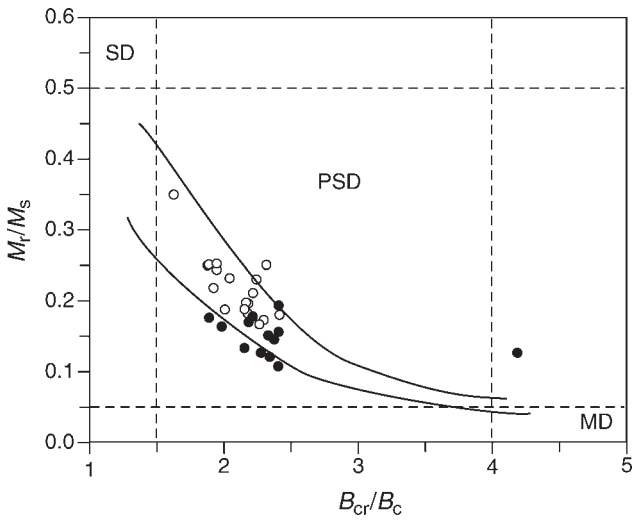

Figure M50 An example of a so-called Day plot. The solid lines represent the experimental calibration by Day *et al.* (1977). SD, single domain; PSD, pseudosingle-domain; MD, multidomain. Data points are from Icelandic lava with stable (open circles) and unstable (closed circles) behavior of the natural remanent magnetization. Dunlop (2002) showed that SP grains plot upward and to the right of the calibrated band.

conforms to the new situation rapidly (= on laboratory timescale). At room temperature, magnetite grains smaller than 20–25 nm in size are superparamagnetic. Single-domain grains contain one magnetic domain and are paleomagnetically most stable (25–80 nm). The stability can be expressed in terms of relaxation time. Pseudosingle-domain grains (80 nm—~10–15 μm) contain "a few" domains (up to ~10); they are paleomagnetically very stable. Multidomain grains (>10–15 μm) contain many domains (>~10); they are paleomagnetically less stable.

The number of domains is a function of the grain's size and shape, and of the saturation magnetization of the magnetic material. In essence, a grain of a material with a high-saturation magnetization like magnetite will contain (much) more domains than a grain with the same size but of material with a low-saturation magnetization like hematite (see Table M3). Therefore we need to know the magnetic mineralogy before we can make a proper grain-size estimate with magnetic methods. Macroscopically, the domain state is reflected in the so-called hysteresis loop (Figure M49 left and central panels), the response of a sample to a cyclic applied magnetic field. If remanent magnetization occurs, the loops are open (the surface area corresponds to the energy contained in the magnetic system). The maximum value of the magnetization is the saturation magnetization (M_s or σ_s), the corresponding remanent magnetization (when the external field is reduced to zero) is termed the remanent saturation magnetization (SIRM or saturation isothermal remanent magnetization, also M_{rs} or σ_{rs}). The field values where M is zero are termed coercive force (B_c or H_c). The field value where the remanence corresponds to zero is labeled remanent coercive force (B_{cr} or H_{cr}, cf. Figure M49 right panel). B_c and B_{cr} go up with decreasing grain size. The M_{rs}/M_s and B_{cr}/B_c ratios are grain-size indicative, their plot against each other is referred to as "Day" plot (Figure M50). Ferro- and ferrimagnetic materials have lower values for their coercive forces than antiferromagnetic materials (see Table M3). Minerals with low coercivity values are termed magnetically "soft" while those with high values are "hard."

It is important to note that coercive force values are concentration independent when magnetic interaction can be neglected. To a first-order description, this is warranted in many natural situations. Under this condition, values of magnetizations and various remanences scale linear with the concentration of the magnetic mineral. By dividing two concentration-dependent parameters, a concentration-independent ratio is obtained that contains information on grain size or the oxidation degree of the magnetic mineral. This idea of correcting for concentration forms the basis of many magnetic proxies.

Magnetic proxy parameters

The concept of using magnetic properties as proxy parameters and correlation tool in a geoscientific context was put forward in the late 1970s mostly by Oldfield and his coworkers; the article in *Science* (Thompson *et al*., 1980) is often considered as the formal definition of "environmental magnetism" as a subdiscipline. Before briefly highlighting some magnetic proxies, we need to introduce two other important mineral-magnetic parameters, the low-field or initial susceptibility (χ_{in} or κ_{in}) and the anhysteretic remanent magnetization (ARM).

The initial susceptibility is the magnetization of a sample in a small applied field (up to a few times the intensity of the geomagnetic field, 30–60 μT) divided by that field. Measurement takes a few seconds and requires no specific sample preparation; instrumentation is sensitive. This makes initial susceptibility an attractive proxy parameter, especially for correlation purposes. All materials have a magnetic susceptibility, also paramagnets and diamagnets. The initial susceptibility

Table M3 Saturation magnetization, typical coercive forces, remanent coercive forces and field required to reach saturation of some magnetic minerals (at room temperature)

Mineral	Saturation magnetization (A m^2 kg^{-1})	Coercive force[a] (mT)	Remanent coercive force[a] (mT)	Saturation field (T)
Magnetite	92[b]	5–80	15–100	<0.3[c]
Maghemite	~65–74[c]	5–80	15–100	<0.3[d]
Hematite	0.1–0.4	100–500	200–800	~1–~5
Iron	217	<1–10	~5–15	<0.1[d]
Goethite	0.01–1	>1000	>2000	~10–>20
Pyrrhotite	18	8–100	9–115	up to 1[d]
Greigite	~30[e]	15–40	35–70	<0.3[d]

[a]In the indicative ranges given the smallest number refers to multidomain particles and the largest to single-domain particles. Needle-shaped particles of strong magnetic material can have higher values for the coercivity than quoted in the ranges above.
[b]With increasing substitution of Ti, the saturation magnetization decreases.
[c]The ideal maghemite composition has a saturation magnetization of 74 A m^2 kg^{-1}, in practice lower values are often determined.
[d]Oxidized coatings and differential composition often increase coercivity and fields in which saturation is reached.
[e]The purity of greigite samples is problematic, the saturation magnetization value should be considered a minimum.

Table M4 Some important magnetic proxy parameters

Parameter/ratio	Name	Indicative of
χ_{in}	Low-field susceptibility	Combination of ferromagnetism, paramagnetism, and diamagnetism; ferromagnetism (s.l.) when concentration of ferrimagnets is >1%
χ_{hifi}	High-field susceptibility	Paramagnetism and diamagnetism
χ_{ferri}	Ferrimagnetic susceptibility	Ferro-/ferrimagnetism ($=\chi_{in}-\chi_{hifi}$)
χ_{ARM}	Anhysteretic susceptibility	Single-domain material, particularly magnetite and maghemite
HIRM	Hard IRM	Antiferromagnetic minerals: hematite and goethite
S	*S*-ratio	"Soft" IRM/"hard" IRM; "magnetite"/ "hematite" ratio in terms of magnetic remanence
ARM/SIRM		Grain size
SIRM/χ_{in}		Grain size, for low SIRM values concentration influence as well. Magnetic sulfides have high values
ARM/χ_{in}		Grain size
M_{rs}/M_s		Grain size
B_{cr}/B_c		Grain size
M_s/χ_{ferri}		Superparamagnetic material
χ_{FD}%	Frequency dependence of susceptibility $((\chi_{lowfreq}-\chi_{highfreq})/\chi_{lowfreq})*100\%$	Senses window in the superparamagnetic grain-size range, instrumentally dictated

of a geologic sample is therefore a composite of the diamagnetic, paramagnetic, and ferromagnetic (*sensu lato*) contributions, something which should be kept in mind when interpreting susceptibility profiles. Ferro- and ferrimagnetic materials have very high initial susceptibilities so that for concentrations larger than ~1% the measured susceptibility may be equated to the ferromagnetic susceptibility. For lower concentrations—the rule in sediment and soil samples—the paramagnetic and diamagnetic contributions can be substantial. Superparamagnetic grains have a high value for the initial susceptibility, much higher than the bulk value of the same material. The variation of initial susceptibility with grain size is small for single domain and larger grains. The superparamagnetic threshold size is dependent on the measurement frequency. By measuring at different frequencies the frequency dependence of the initial susceptibility can be calculated. This is a proxy for the relative amount of superparamagnetic grains.

The ARM is induced by an asymmetric alternating field, which is reduced from a peak value to zero. Often equipment for alternating field demagnetization is used, the asymmetry is created by a small direct current bias field. Typical values for the peak alternating field are 100–300 mT, whereas the bias field can vary between 30 and 100 μT. The ARM intensity is a function of the bias field, for low bias fields (say <100 μT) it scales linearly. Hence, by dividing the ARM intensity by the bias field value, a field-independent parameter is created, referred to as ARM susceptibility (χ_{ARM}) through its analogy with the low-field susceptibility. Some instruments allow to have the bias field switched on in desired windows of the decreasing alternating field to sense particular coercivity windows, such ARMs are referred to as partial ARM, labeled pARM. ARM is considered to be a good analog of thermoremanent magnetization created by cooling through the Curie temperature in a small magnetic field. Single-domain grains are sensed in particular by ARM.

Most proxy parameters are based on combinations of low-field susceptibility and/or various remanent magnetizations because they are most quickly measured (measurement of a complete hysteresis loop still takes 3 min on dedicated instrumentation, operator attendance is, however, required). Instrumentation that can measure ARMs and IRMs in a fully automated fashion has meanwhile developed, a distinct advantage (Table M4).

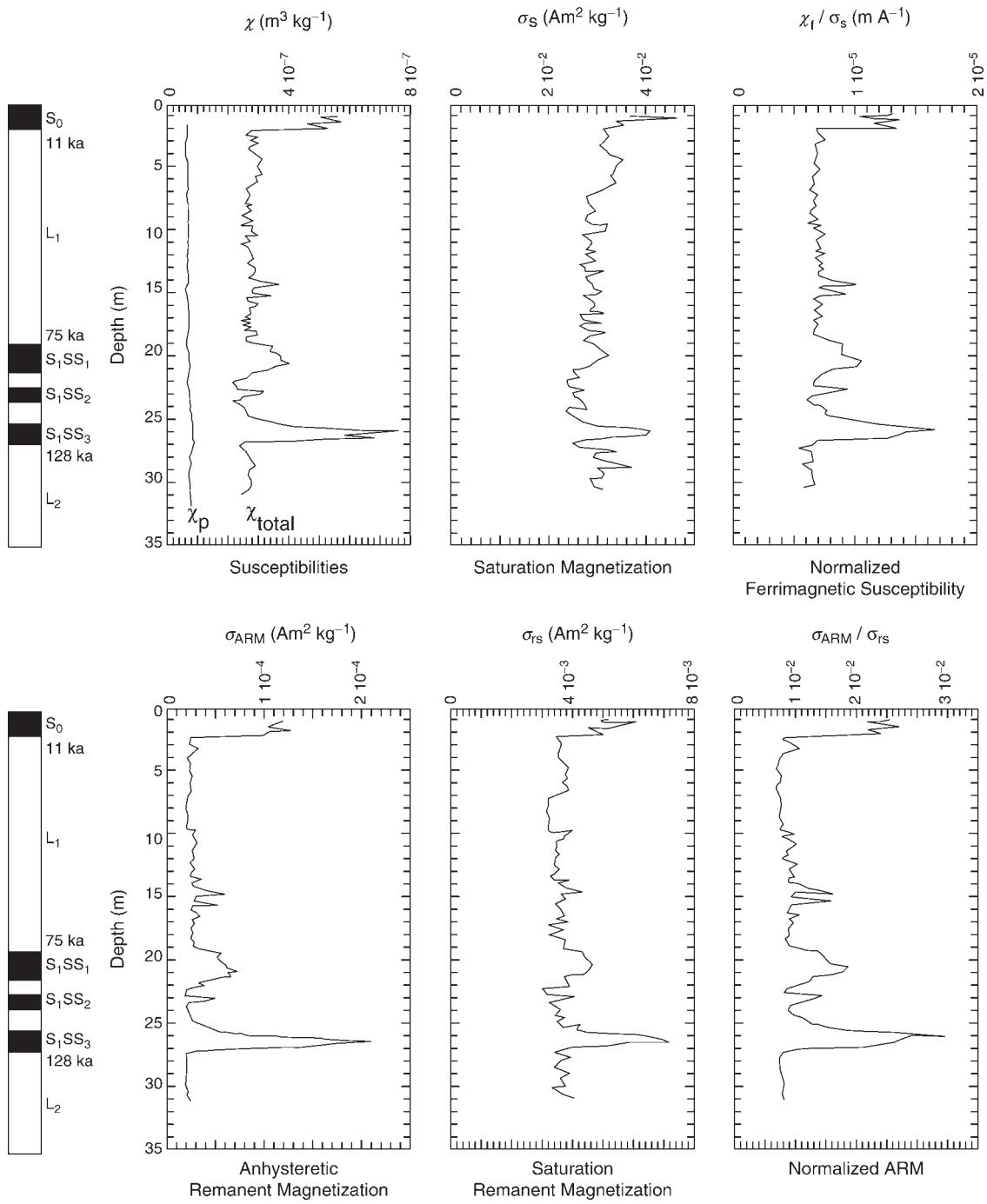

Figure M51 Magnetic properties from the last 140 ka of a loess–paleosol sequence at Xining, western Loess Plateau, China (simplified after Hunt *et al.* 1995). (a) (*Outermost left*): Lithological column with ages for the paleosols. *S*, soil; *L*, loess, numbering starts from the Holocene soil S_0. In the S_1 complex three subunits are distinguished: SS_1, SS_2, and SS_3. (*Left-hand panel*): Susceptibility. χ_p, the susceptibility of paramagnetic minerals (measured in a high-magnetic field), appears to be relatively constant in this profile. χ_{total} refers to the low-field susceptibility. The ferrimagnetic contribution to the low-field susceptibility equals $\chi_{total}-\chi_p$. (*Central panel*): Saturation magnetization which is used as a normalizer to remove concentration effects. (*Right-hand panel*): The ratio χ_f/σ_s, indicative of SP grains, increases in the paleosols. It is also slightly increased in a zone in L_1, which probably indicates a warmer period in the glacial period in which L_1 was deposited. Note that no soil is visually evident in this zone. (b) (*Outermost left*): see Figure M51 (*Left-hand panel*): ARM intensity expressed on a mass-specific basis (σ_{ARM}). ARM values are higher in soils than in loess. (*Central panel*): SIRM intensity expressed on a mass-specific basis (σ_{rs}). Note that the pattern is noisier than that of the ARM and that is differs from that of σ_s (see a) above. (*Right-hand panel*): Higher ratios of σ_{ARM}/σ_r indicate greater abundances of SD and PSD particles in the soils. Not only the SP fraction, but also the SD and the PSD fractions increase in soils. Subtle paleoclimatic variations can also be traced within and between lithological units, e.g., paleosol S_1SS_3 is much more developed than S_1SS_1 and, in particular, than S_1SS_2. The climate change which led to the formation of the present-day soil, S_0, was apparently sharp because no intermediate values (such as for S_1SS_3) are present.

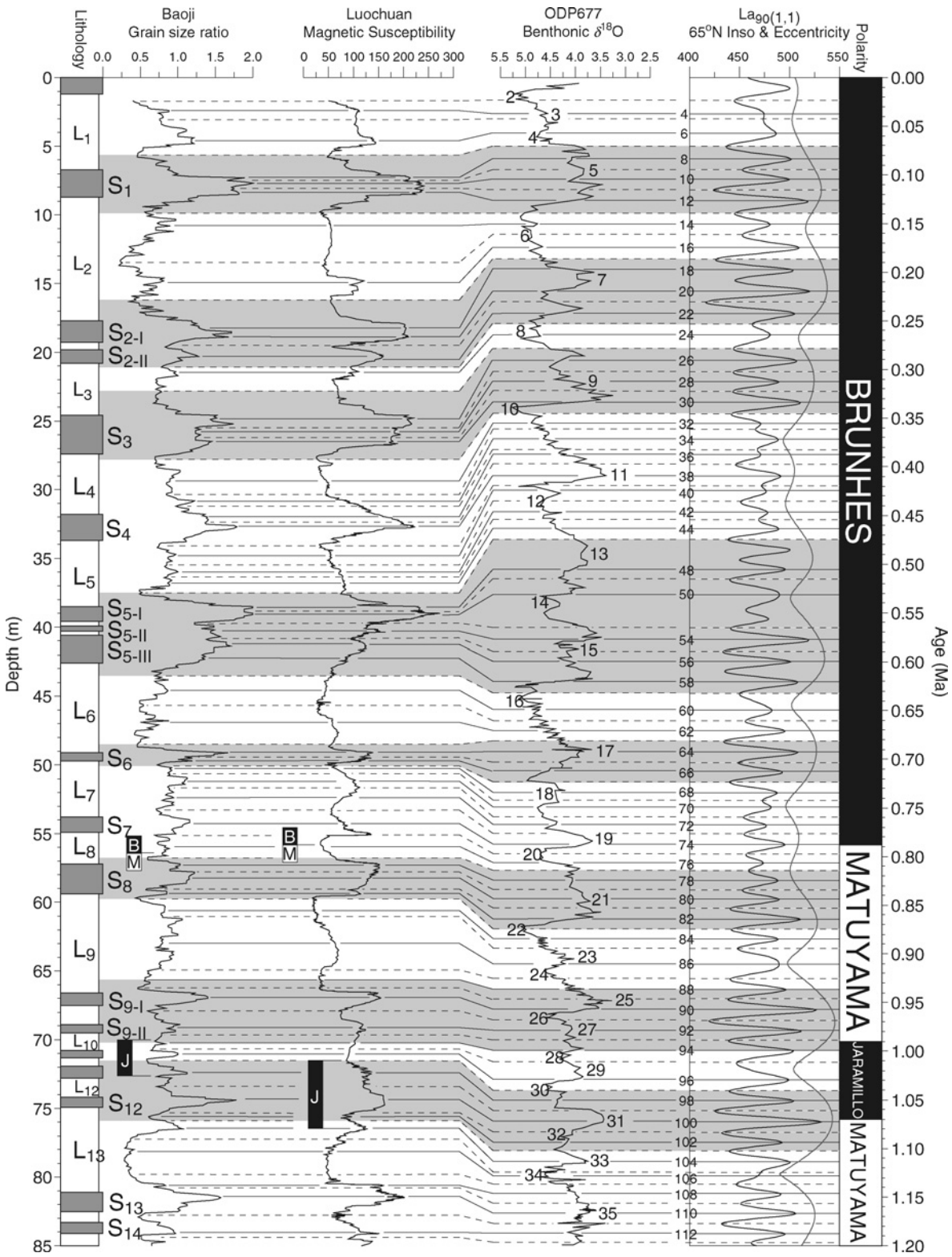

Figure M52 Correlation of the Baoji grain-size ratio (<2 μm (%)/>10 μm (%)) and Luochan low-field magnetic susceptibility (χ_{in}; fitted to the Baoji depth scale) to the 65° N insolation curve of Laskar (1990) (i-cycle numbers shown on the left) and the ODP677 benthonic $\delta^{18}O$ record (Marine isotope stages adjacent to curve). The eccentricity component from the Laskar (1990) solution is displayed for comparison with the longer term trends observed within the loess record. Correlation points linking warm features are shown with full lines while those for cold features are shown with dashed lines.

Some examples

The loess–paleosol climate archive was studied numerous times since Heller and Liu (1982) reported reliable magnetostratigraphic data from the Chinese Loess Plateau (CLP). The climatic conditions on the CLP are broadly determined by the relative intensities of the summer and winter monsoons. The summer monsoon delivers moisture toward the CLP, so strong summer monsoons indicate a wetter (and warmer) climate whereas strong winter monsoons (more and coarser dust) herald dry and cold climate conditions. Hunt *et al*. (1995b) utilized the magnetic proxy approach to highlight subtle differences within loess–paleosol profiles on the CLP (see Figure M51). Mainly qualitative observations in the loess-soil profile were confirmed whereas very subtle differences within the loess horizons were detected. Soils that are indicative for a wetter climate are characterized by higher values for χ_{in}, in line with earlier observations. By using χ_{in} as proxy for the intensity of the summer monsoon and the grain-size ratio as proxy for the winter monsoon, Heslop *et al*. (2000) were able to tune the entire "yellow" loess record (2.6 Ma) to the astronomical solution of Laskar (1990) providing a high-resolution timescale for the loess–paleosol deposits (Figure M52). With this high-resolution timescale, climatic and environmental changes can be put into a regional and also global perspective.

Mineral-magnetic proxy studies from the marine realm are numerous as well. Many studies report on the sensitivity of magnetic proxies to climate change since the mid-1980s. Robinson (1986) showed for North Atlantic sediments fairly close to the Mid-Atlantic spreading ridge west from Spain that concentration-dependent and -independent magnetic parameters and ratios reflect changes in climate caused by changes in provenance of the sediment flux. He argued for an eolian source and found indications for ice-rafted debris. Later work among others by Stoner and colleagues (1996) documented the sensitivity of North Atlantic sediments, in particular from higher latitudes, to record Heinrich events, short-duration rapid climate variations. The minor importance of reductive diagenetic processes in most of these sediments and distinct magnetic properties of the source areas allow interpretation of subtle variations in the record in terms of climate change. Reductive diagenesis obscures the magnetic fingerprint of source areas (e.g., Bloemendal *et al*., 1992). The presence of pyrite (FeS_2) and magnetic sulfides testifies anoxic conditions. Joint mineral-magnetic and geochemical analysis can be used to evaluate the extent of diagenesis (e.g., Dekkers *et al*., 1994; Passier *et al*., 2001). Oxidative diagenesis has a typical magnetic signature (Passier *et al*., 2001), which was utilized by Larrasoaña *et al*. (2003a) to provide a proxy for bottom-water ventilation in the Mediterranean Sea during sapropel formation (Figure M53). They distinguish three types of sapropel environment: (i) sapropels without oxidation fronts with high organic matter contents inferred to be deposited under severely anoxic conditions; (ii) sapropels with both dissolution and oxidation fronts, the mostly occurring situation referred to as "anoxic"; and (3) sapropels without dissolution front but with a well-developed oxidation front, referred to as "less anoxic." The third group implies no excess sulfide being generated within the sapropel for a dissolution front formed below it. These sapropels are most prone to be reoxidized completely and therefore easily escape visual detection. They can, however, be traced with magnetic (and other) proxies.

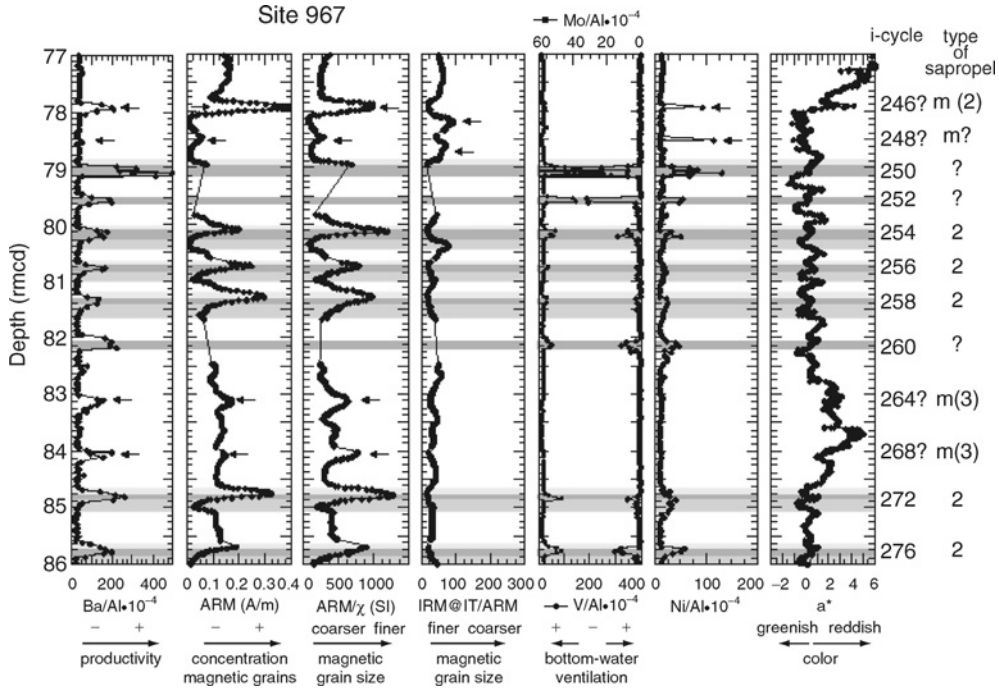

Figure M53 A series of geochemical and magnetic proxies measured on samples from ODP Site 967 (Eastern Mediterranean) with their meaning underneath the abscissas (after Larrasoaña *et al.*, 2003a). Sediments constitute an alternation of marly limestones and marls with sapropels intercalated (sapropels are sediments with more than 2% organic matter and therefore dark-brown to black colored). Sapropeletic sediments are indicated by darkest gray shading, dissolution zones with intermediate gray, and reoxidized zones with lightest gray. The insolation cycle (i-cycle) codification implies an age range from ~2.9 to ~2.5 Ma. The sapropels class into groups (2) and (3). Arrows indicate the position of completely reoxidized (missing, m) sapropels on the basis of magnetic and geochemical proxies. In cases where assignment to a sapropel type is not certain because of lack of magnetic data due to unavailability of the core segment for rock magnetic analysis, a question mark is put.

Mixed magnetic mineralogy, magnetic interaction, and thermal relaxation

Often magnetite-like minerals dominate the magnetic signal. However, more detailed analysis has shown that the occurrence of mixed magnetic mineralogy is the rule rather than the exception. The absolute values of HIRM ("hard" IRM) as an indicator for the amount of hematite have been used as a proxy for dust input by Larrasoaña *et al*. (2003b). They gave the samples at 0.9 T IRM which was demagnetized at 120 mT peak AF to cope with the limited dynamic range of the magnetometer.

Also the *S*-ratio is an example of a parameter to distinguish between "magnetite" and "hematite" ("soft" IRM and "hard" IRM; with respect to a saturating forward IRM and various back field IRMs). In particular, S_{300} is being used as indicator for the magnetite–hematite ratio. S_{300} equals 1 (or −1 depending on the definition, see Bloemendal *et al*., 1992 and Kruiver and Passier, 2001) would represent magnetite only and that lower values would indicate the presence of hematite. Magnetite fully saturates in a 300 mT field and hematite is (much) harder, yielding lower *S*-ratios. Up to now, the ratio has been used as a qualitative indicator only. The interpretation of the S_{300} in terms magnetite and hematite has been criticized by Kruiver and Passier (2001) who modelled that for oxidized magnetite the forward S_{300} would yield values lower than one and that when more than two magnetic minerals are present the *S*-ratio can be seriously flawed. So, the meaning of lower *S*-ratios needs to be assessed on a case-by-case basis.

Another way to quantify mixed magnetic mineralogy is the so-called IRM component analysis, the decomposition of a measured IRM acquisition curve into several components with the use of model functions. Initially, cumulative log–Gaussian curves were used based on the experimental observation by Robertson and France (1994) that such curves closely conform to measured IRM acquisition curves. Kruiver *et al*. (2001) proposed the use of the *F*-test (and *t*-test where appropriate) to judge upon the number of coercivity fractions required for an optimal fit from a statistical viewpoint. The cumulative

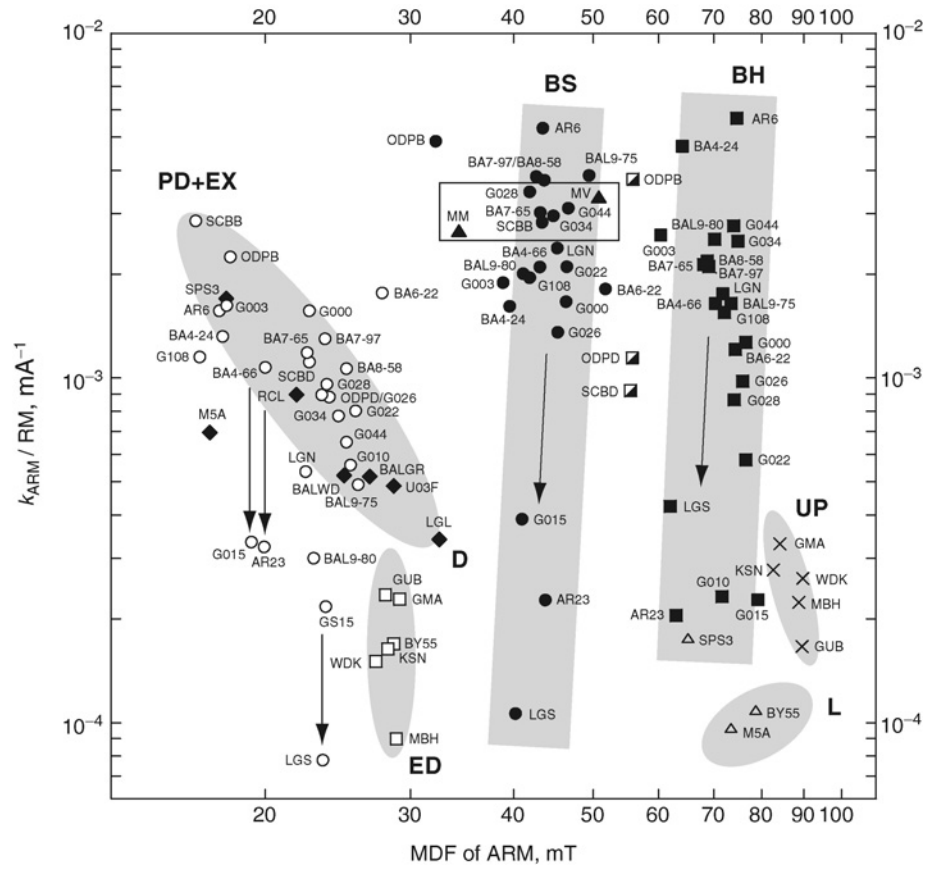

Figure M54 Magnetic fingerprint diagram of MDF_{ARM} vs k_{ARM}/IRM (after Egli, 2004). Summary of the magnetic properties of ARM (300 mT peak AF, 0.1 mT bias field) and IRM (300 mT acquisition field to avoid magnetization that cannot be AF demagnetized) for all iron spinel components identified by Egli (2004). The magnetic components group into different clusters, indicated by gray ellipses and rectangles. White letters classify all components into low-coercivity magnetosomes (biogenic soft, BS: dots), high-coercivity magnetosomes (biogenic hard, BH: squares), ultrafine extracellular magnetite (EX: circles), pedogenic magnetite (PD: diamonds), detrital particles transported in water systems (D: diamonds), windblown particles (eolian dust, ED: open squares), atmospheric particulate matter produced by urban pollution (UP: crosses), and a maghemite component in loess (L: open triangles). Other components, as BM (dots) and BI (half-filled squares), have been measured in a few samples only and are not labeled. The open rectangle indicates the range of values measured in samples of cultured magnetotectic bacteria (triangles). GS15 labels the measurement of extracellular magnetite particles produced by a cultured dissimilatory iron-reducing microorganism. Its properties are influenced by the strong magnetostatic interactions within clumps of these particles which form spontaneously during the sample preparation. Smaller values of MDF_{ARM} and larger values of k_{ARM}/IRM are expected for these particles when they are dispersed in natural sediments: in this case, GS15 would probably fall into the cluster labeled with PD+EX. Arrows indicate the decrease of k_{ARM}/IRM observed during anoxic conditions in lake sediments.

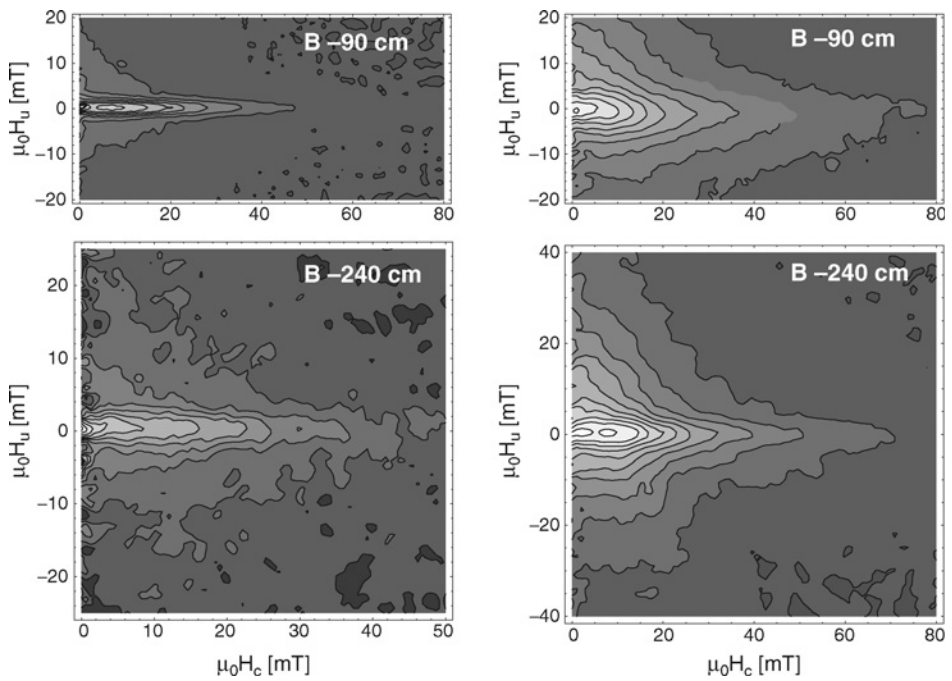

Figure M55 FORC diagrams of paleosols (*top panels*) and loesses (*bottom panels*) from Moravia (Czech Republic) before (*left panels*) and after three times ferrous iron acid-ammonium–oxalate extraction (*right panels*) to dissolve the finest magnetite particles (after Van Oorschot *et al.*, 2002). After extraction, coercivity maxima shift toward the right, indicating dissolution of the finest particles.

log–Gaussian model function would be valid in the absence of magnetic interaction. Egli (2003) extended the use of the model functions to a set of skewed generalized Gaussian functions where skewness and kurtosis are additional free parameters. He showed that many natural samples would require skewed model functions for optimal fits (kurtosis appeared to be not significant). Heslop *et al*. (2004) utilized Preisach modeling to document that thermal relaxation and magnetic interaction would yield negatively skewed distributions already for low levels of interaction and thermal relaxation supporting the observations of Egli (2003, 2004). In Figure M54, the summary diagram of Egli (2004) is reproduced. He processed a series of lake sediments, marine sediments, soils, loesses, polluted samples, and magnetotactic and extracellular bacteria with the procedure described by Egli (2003). He concluded that a plot of the median destructive field (MDF, the peak alternating field strength at which 50% of a remanent magnetization is demagnetized) of the ARM vs the ARM susceptibility divided by the IRM discriminates the grouping most instructively. In many natural samples combinations of these groups are present and observed variability could be described meaningfully by these "endmember groups." It should be kept in mind that the low IRM peak acquisition field (300 mT) used in the approach excludes hematite, goethite, and other antiferromagnets from the analysis.

A nice way to illustrate the occurrence of magnetic interaction is by the so-called first-order reversal curve (FORC) plots (Figure M55), an approach introduced into environmental magnetism by Pike *et al*. (1999) and Roberts *et al*. (2000). On the abscissa coercivity is plotted, whereas on the ordinate magnetic interaction is expressed. Zero magnetic interaction occurs when $\mu_0 H_u$ equals zero, most contour density in this area in the samples before sequential extraction implies minor interaction which was taken by Van Oorschot *et al*. (2002) that IRM component analysis was warranted. The plots are normalized.

Proxy for anthropogenic pollution

A number of studies have produced reasonable correlations between magnetic proxy parameters, in particular low-field susceptibility, and a series of contaminants, either of organic or of inorganic chemical origin. The underlying reason for the magnetic methods to yield fairly consistent results under certain conditions is the sorption capacity of fine-grained iron oxides and sulfides. For airborne particulate matter—for example from industrial fly ash, general industrial activity, or urban traffic—magnetic parameters may provide an estimate of the pollution load (e.g., Dekkers and Pietersen, 1992; Morris *et al*., 1995; Matzka and Maher, 1999; Xie *et al*., 2001; Muxworthy *et al*., 2002). The suitability of magnetic parameters for monitoring of pollution loads in some central European countries has been investigated by the MAGPROX team. In a number of settings magnetic susceptibility is a good indicator of atmospherically derived particulate matter. A recent example of the magnetic expression of the dust load in tree leaves includes the work by Hanesch *et al*. (2003), the impact of an industrial zone could be evaluated straightforwardly. In the same area, a province in Austria, heavy metal concentrations in soils could be traced magnetically by low-field susceptibility patterns (Hanesch and Scholger, 2002).

Summary

Subtle changes in magnetic properties reflect changes in magnetic mineralogy, grain size, oxidation degree, stoichiometry, strain state, etc. These can be understood and explained in terms of changing provenance areas, climatic conditions, diagenetic regimes, and—under certain conditions—anthropogenic pollution. Therefore, combined with analytical assets: sensitivity, rapidity, nondestructiveness, and comparative ease of sample preparation, they are an attractive set of proxy parameters. The interpretive value can be enhanced by utilizing several magnetic proxies together with a few geochemical proxies, for example, elemental analysis. Increased use of magnetic proxies is foreseen as a consequence of methodological advances in unraveling mixed magnetic mineralogy and further establishment of more quantitatively based parameters.

M.J. Dekkers

Bibliography

Bloemendal, J., King, J.W., Hall, F.R., and Doh, S.-J., 1992. Rock magnetism of Late Neogene and Pleistocene deep-sea sediments: relationship to sediment source, diagenetic processes, and sediment lithology. *Journal of Geophysical Research*, **97**: 4361–4375.

Day, R., Fuller, M., and Schmidt, V.A., 1977. Hysteresis properties of titanomagnetites: grain-size and compositional dependence. *Physics of the Earth and Planetary Interiors*, **13**: 260–267.

Dekkers, M.J., Langereis, C.G., Vriend, S.P., van Santvoort, P.J.M., and de Lange, G.J., 1994. Fuzzy *c*-means cluster analysis of early diagenetic effects on natural remanent magnetisation acquisition in a 1.1 Myr piston core from the Central Mediterranean. *Physics of the Earth and Planetary Interiors*, **85**: 155–171.

Dekkers, M.J., and Pietersen, H.S., 1992. Magnetic properties of low-Ca fly ash: a rapid tool for Fe-assessment and a proxy for environmental hazard. In Glasser, F.P. *et al*. (eds.), *Advanced Cementitious Systems: Mechanisms and Properties, Material Research Society Symposium Proceedings*, **245**: 37–47

Dunlop, D.J., 2002. Theory and application of the Day plot (M_{rs}/M_s versus H_{cr}/H_c) 1. Theoretical curves and tests using titanomagnetite data. *Journal of Geophysical Research*, **107**: doi: 10.1029/2001JB000486.

Dunlop, D.J., and Özdemir, Ö., 1997. *Rock Magnetism: Fundamentals and Frontiers.* Cambridge:Cambridge University Press, 573 pp.

Egli, R., 2003. Analysis of the field dependence of remanent magnetisation curves. *Journal of Geophysical Research*, **108**: doi:10.1029/2002JB002023.

Egli, R., 2004. Characterization of individual rock magnetic components by analysis of remanence curves. 1. Unmixing natural sediments. *Studia Geophysica et Geodaetica*, **48**: 391–446.

Evans, M.E., and Heller, F., 2003. *Environmental Magnetism—Principles and Applications of Enviromagnetics.* San Diego: Academic Press, 299 pp.

Hanesch, M., and Scholger, R., 2002. Mapping of heavy metal loadings in soils by means of magnetic susceptibility measurements. *Environmental Geology*, **42**: 857–870.

Hanesch, M., Scholger, R., and Rey, D., 2003. Mapping dust distribution around an industrial site by measuring magnetic parameters of tree leaves. *Atmospheric Environment*, **37**: 5125–5133.

Heller F., and T.-S., Liu 1982. Magnetostratigraphical dating of loess deposits in China. *Nature*, **300**: 431–433.

Heslop, D., Langereis, C.G., and Dekkers, M.J., 2000. A new astronomical timescale for the loess deposits of Northern China. *Earth and Planetary Science Letters*, **184**: 125–139.

Heslop, D., McIntosh, G., and Dekkers, M.J., 2004. Using time- and temperature-dependent Preisach models to investigate the limitations of modelling isothermal remanent magnetization acquisition curves with cumulative log Gaussian functions. *Geophysical Journal International*, **157**: 55–63.

Hunt, C.P., Moskowitz, B.M., and Banerjee, S.K., 1995. Magnetic properties of rock and minerals. In Ahrens, T.J. (ed.), *Rock Physics and Phase Relations: A Handbook of Physical Constants*, Vol. 3. American Geophysical Union, pp. 189–204.

Hunt, C.P., Banerjee, S.K., Han, J., Solheid, P.A., Oches, R., Sun, W., and Liu, T., 1995b. Rock-magnetic properties of climate change in the loess–paleosol sequences of the western Loess Plateau of China. *Geophysical Journal International*, **123**: 232–244.

Kruiver, P.P., Dekkers, M.J., and Heslop, D., 2001. Quantification of magnetic coercivity components by the analysis of acquisition curves of isothermal remanent magnetisation. *Earth and Planetary Science Letters*, **189**: 269–276.

Kruiver, P.P., and Passier, H.F., 2001. Coercivity analysis of magnetic phases in sapropel S1 related to variations in redox conditions, including an investigation of the *S*-ratio. *Geochemistry Geophysics Geosystems*, **2**(12): doi:10.1029/2001GC000181.

Larrasoaña, J.C., Roberts, A.P., Stoner, J.S., Richter, C., and Wehausen, R., 2003a. A new proxy for bottom-water ventilation in the eastern Mediterranean based on diagenetically controlled magnetic properties of sapropel-bearing sediments. *Palaeogeography Palaeoclimatology Palaeoecology*, **190**: 221–242.

Larrasoaña, J.C., Roberts, A.P., Rohling, E.J., Winklhofer, M., and Wehausen, R., 2003b. Three million years of monsoon variability over the Northern Sahara. *Climate Dynamics*, **21**: 689–698.

Laskar, J., 1990. The chaotic motion in the solar system: a numerical estimate of the size of the chaotic zones. *Icarus*, **88**: 266–291.

MAGPROX network. http://www.uni-tuebingen.de/geo/gpi/ag-appel/projekte/envmag/magprox/index.html

Maher, B.A., and Thompson, R. (eds.), 1999. *Quaternary Climates, Environments and Magnetism.* Cambridge: Cambridge University Press, 390 pp.

Matzka, J., and Maher, B.A., 1999. Magnetic biomonitoring of roadside tree leaves: identification of spatial and temporal variations in vehicle-derived particulates. *Atmospheric Environment*, **33**: 4565–4569.

Morris, W.A., Versteeg, J.K., Bryant, D.W., Legzdins, A.E., McCarry, B.E., and Marvin, C.H., 1995. Preliminary comparisons between mutagenicity and magnetic susceptibility of respirable airborne particulate. *Atmospheric Environment*, **29**: 3441–3450.

Muxworthy, A.R., Schmidbauer, E., and Petersen, N., 2002. Magnetic properties and Mössbauer spectra of urban atmospheric particulate matter: a case study from Munich, Germany. *Geophysical Journal International*, **150**: 558–570.

Passier, H.F., de Lange, G.J., and Dekkers, M.J., 2001. Rock-magnetic properties and geochemistry of the active oxidation front and the youngest sapropel in the Mediterranean. *Geophysical Journal International*, **145**: 604–614.

Pike, C.R., Roberts, A.P., and Verosub, K.L., 1999. Characterizing interactions in fine magnetic particle systems using first order reversal curves. *Journal of Applied Physics*, **85**: 6660–6667.

Roberts, A.P., Pike, C.R., and Verosub, K.L., 2000. FORC diagrams: a new tool for characterizing the magnetic properties of natural samples. *Journal of Geophysical Research*, **105**: 28461–28475.

Robertson, D.J., and France, D.E., 1994. Discrimination of remanence-carrying minerals in mixtures, using isothermal remanent magnetisation acquisition curves. *Physics of the Earth and Planetary Interiors*, **82**: 223–234.

Robinson, S., 1986. The late Pleistocene palaeoclimatic record of North Atlantic deep-sea sediments revealed by mineral-magnetic measurements. *Physics of the Earth and Planetary Interiors*, **42**: 22–47.

Stoner, J.S., Channell, J.E.T., and Hillaire- Marcel, C., 1996. The magnetic signature of rapidly deposited detrital layers from the deep Labrador Sea: relationship to North Atlantic Heinrich Layers, *Paleoceanography*, **11**: 309–325.

Thompson, R., Bloemendal, J., Dearing, J.A., Oldfield, F., Rummery, T.A., Stober, J.C., and Turner, G.M., 1980. Environmental applications of magnetic measurements. *Science*, **207**: 481–486.

Van Oorschot, I.H.M., Dekkers, M.J., and Havlicek, P., 2002. Selective dissolution of magnetic iron oxides with the acid-ammonium-oxalate/ferrous-iron extraction technique-II. Natural loess and palaeosol samples. *Geophysical Journal International*, **149**: 106–117.

Xie, S., Dearing, J.A., Boyle, J.F., Bloemendal, J., and Morse, A.P., 2001. Association between magnetic properties and element concentrations of Liverpool street dust and its implications. *Journal of Applied Geophysics*, **48**: 83–92.

Cross-references

Archeology, Magnetic Methods
Biomagnetism
Environmental Magnetism
Paleointensity, Relative, in Sediments
Paleomagnetism
Rock Magnetism

http://www.springer.com/978-1-4020-3992-8

Encyclopedia of Geomagnetism and Paleomagnetism
Gubbins, D.; Herrero-Bervera, E. (Eds.)
2007, XXVI, 1054 p. 718 illus., 50 illus. in color.,
Hardcover
ISBN: 978-1-4020-3992-8